Research Article

ADVANCED PHOTONICS

Orbital angular momentum based intra- and interparticle entangled states generated via a quantum dot source

Alessia Suprano,[a] Danilo Zia,[a] Mathias Pont,[b] Taira Giordani,[a] Giovanni Rodari,[a] Mauro Valeri,[a] Bruno Piccirillo,[c,d] Gonzalo Carvacho,[a] Nicolò Spagnolo,[a] Pascale Senellart,[b] Lorenzo Marrucci,[c] and Fabio Sciarrino[a,*]

[a]Sapienza Università di Roma, Dipartimento di Fisica, Roma, Italy
[b]Université Paris-Saclay, UMR 9001, Centre for Nanosciences and Nanotechnology, CNRS, Palaiseau, France
[c]Università di Napoli Federico II, Complesso Universitario di Monte Sant'Angelo, Dipartimento di Fisica "Ettore Pancini", Napoli, Italy
[d]INFN - Sezione di Napoli, Napoli, Italy

Abstract. Engineering single-photon states endowed with orbital angular momentum (OAM) is a powerful tool for quantum information photonic implementations. Indeed, due to its unbounded nature, OAM is suitable for encoding qudits, allowing a single carrier to transport a large amount of information. Most of the experimental platforms employ spontaneous parametric down-conversion processes to generate single photons, even if this approach is intrinsically probabilistic, leading to scalability issues for an increasing number of qudits. Semiconductor quantum dots (QDs) have been used to get over these limitations by producing on-demand pure and indistinguishable single-photon states, although only recently they have been exploited to create OAM modes. Our work employs a bright QD single-photon source to generate a complete set of quantum states for information processing with OAM-endowed photons. We first study hybrid intraparticle entanglement between OAM and polarization degrees of freedom of a single photon whose preparation was certified by means of Hong–Ou–Mandel visibility. Then, we investigate hybrid interparticle OAM-based entanglement by exploiting a probabilistic entangling gate. The performance of our approach is assessed by performing quantum state tomography and violating Bell inequalities. Our results pave the way for the use of deterministic sources for the on-demand generation of photonic high-dimensional quantum states.

Keywords: orbital angular momentum; quantum dot; intraparticle entanglement; interparticle entanglement; Bell violation.

Received Feb. 8, 2023; revised manuscript received Jun. 2, 2023; accepted for publication Jul. 31, 2023; published online Aug. 30, 2023.

[DOI: 10.1117/1.AP.5.4.046008]

1 Introduction

In the last few decades, structured light states characterized by an on-demand distribution for both field amplitude and phase have gained great interest.[1] Among them, twisted beams carrying orbital angular momentum (OAM) have been the focus of several studies, due to their wide range of applications. As pointed out by Allen et al.,[2] OAM is carried by all the beams that present a phase term of the form $e^{i\ell\phi}$, where ϕ is the azimuthal angle in cylindrical coordinates and ℓ is an unbounded integer. This phase term is responsible for the typical helicoidal wavefront, and each photon shows an OAM equal to $\ell\hbar$.

In the classical domain, the nontrivial phase structure of OAM states is used in several protocols covering a wide number of fields, such as metrology,[3] imaging,[4–6] particle trapping,[7] and communication.[8–14] The unbounded nature of the OAM is instead the basis of its employment in quantum information. Therefore, OAM modes are used in quantum communication,[15–20] cryptography,[21–23] simulation,[24–26] computation, and information processing.[27–29] In particular, OAM-based encoding enlarges the amount of information that a single photon can support, leading to increased security in the communication protocols.[30,31] When

*Address all correspondence to Fabio Sciarrino, fabio.sciarrino@uniroma1.it

the helicoidal wavefront is coupled with a nontrivial distribution of the spin angular momentum (SAM), also known as polarization, a new class of states called vector vortices (VVs) are introduced. Given this peculiar coupling, VV beams turn out to be intrasystem maximally entangled in the OAM and polarization degrees of freedom.[32] As for the OAM modes, VV beams are applied in several areas, both in the classical and quantum regime, such as optical trapping,[33,34] communication,[35,36] computing,[37–45] sensing, and metrology.[46–50] Moreover, knowing the importance of the Hong–Ou–Mandel (HOM) effect[51] and its applicability in quantum information science,[52] the interference behavior between structured photons has also been studied in order to perform increasingly complex tasks.[53–55]

Despite the large number of applications, sources that produce single photons carrying OAM deterministically and with high brightness are still under development.[56] In fact, most of the experimental implementations leverage the production of single photons through spontaneous parametric down-conversion (SPDC) in nonlinear crystals and modulating their states using bulk systems, such as spatial light modulators[57,58] and q-plates,[22,59,60] employing metasurfaces also for generating entangled states in the OAM and polarization degrees of freedom.[61] However, SPDC is intrinsically probabilistic and suffers from a trade-off between the brightness and the purity of the produced single photons. Moreover, since in each process, it is always possible to generate more than one photon, these kinds of sources undermine the security of quantum cryptography schemes.[62] Semiconductor quantum dots (QDs) have emerged as a platform to overcome these limitations. Acting as artificial atoms when resonantly pumped with pulsed lasers, QDs are capable of generating indistinguishable single photons with high brightness in a nearly deterministic fashion.[63–66] However, most of the efforts have been concentrated on the generation of single or entangled states encoding the information in the photons polarization[67–72] or in the temporal domain.[73] Only recently, works exploiting QDs to engineer OAM modes[56] within a prepare-and-measure framework have appeared. In particular, integrated sources based on microring resonators embedded with QDs[56] have been implemented, in which the OAM states encoded in the generated single photons could not be easily manipulated.

At variance with Ref. 56, we exploit commercial QD-based single-photon sources and focus on the development of quantum information processing protocols with VV beams. Specifically, well-known OAM manipulation technologies have been extensively used to develop high-dimensional quantum communication protocols,[18,22] to reach a high flexibility in engineering arbitrary qudit states,[74,75] and to develop simulated processes based on the quantum walk dynamics.[24,25] Here, we combine these technologies with an innovative and nearly deterministic single-photon source, opening the way for further developments of quantum information protocols that take advantage of high-dimensional resources and of the benefits introduced by using QDs. In particular, besides focusing on interfacing between these two kinds of technologies, we go a step forward and study the hybrid entanglement in high-dimensional Hilbert spaces implementing a quantum gate both in the intra- and interparticle regime (Fig. 1). Previously, states characterized by hybrid intraphoton entanglement between the OAM and polarization degree of freedom have been generated via SPDC processes.[18,38,76,77] However, since this kind of source is probabilistic, the state is certified in a heralded configuration that drastically decreases

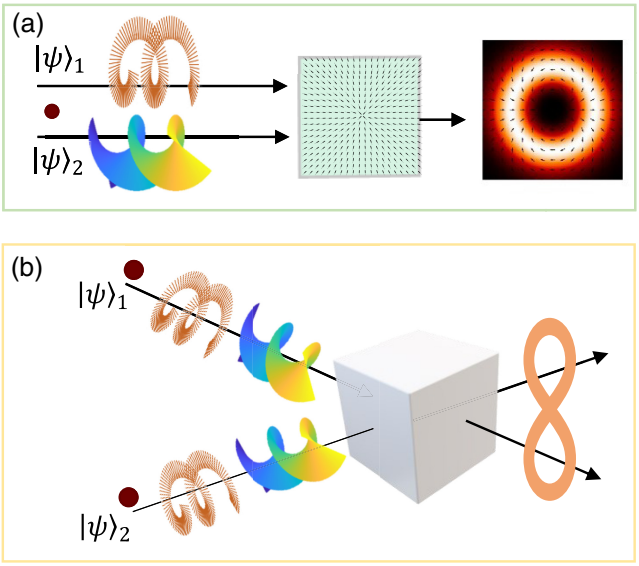

Fig. 1 Entanglement generation. (a) In the intraparticle entanglement, the polarization and OAM subsystems are made to interact using a q-plate. The two-dimensional state $|\psi\rangle_1$ is initialized with the right polarization $|R\rangle = |0\rangle$, while the qudit $|\psi\rangle_2$ is prepared with a null OAM value $|0\rangle$. The action of the unitary operator consists of increasing or decreasing the OAM value in a polarization-dependent way. (b) In the interparticle regime, two photons characterized by defined states in the hybrid space composed of polarization and OAM interfere using a beam splitter. Fixing the elements of the computational basis as $|0\rangle = |L,-2\rangle$ and $|1\rangle = |R,2\rangle$, both $|\psi\rangle_1$ and $|\psi\rangle_2$ are initialized with the qubit state $|0\rangle$, and after postselecting on the coincidence counts a probabilistic entangling quantum gate is implemented. It is worth noting that considering separately the polarization and OAM Hilbert spaces of both photons, the proposed apparatus implements a four-qubit gate.

the generation rate. On the contrary, the employment of a deterministic single-photon source allows us to certify the state directly on the single counts, increasing the generation rate. Moving toward the interparticle regime, QD sources have been proved capable of generating on-demand photons pair entangled in polarization encoding.[78] However, the production of entangled states in different degrees of freedom, such as OAM and radial structure, easily obtained with SPDC sources,[79–81] is still under development. Here, we show a probabilistic approach implementing a gate for an engineer-entangled state in the OAM space. The versatility and flexibility in the generation and manipulation of indistinguishable photons are crucial features for gate implementation. We then move a step forward with respect to Ref. 56 by investigating the indistinguishability of the generated photons and employing a versatile approach. In our platform, the combination of QD-based single-photon sources and well-known OAM manipulation devices allows us to satisfy the aforementioned requirements.

This work is organized as follows. We start by studying the single-photon intraparticle entanglement generation in VV states. By means of q-plate devices,[59,60] we couple the two components of the angular momentum degree of freedom and generate VV beams [Fig. 1(a)]. Then, we move to the multi-photon scenario. Preliminarily, we certify the efficiency of encoding

OAM states on single photons emitted by the QD in different pulses of the pump beam through the evaluation of HOM interference visibility. Thus, we implement a two-photon probabilistic quantum gate, first introduced in Ref. 82, that is able to generate OAM-based entangled photon pairs involving up to four subsystems [Fig. 1(b)]. We verify both the single-photon intraparticle and the two-photon entanglement by performing quantum state tomography and evaluating the Bell inequality in the Clauser–Horne–Shimony–Holt (CHSH) fashion.

2 Experimental Platform

In this section, we preliminarily describe the employed quasi-deterministic single-photon source, by evaluating the intensity autocorrelation and indistinguishability of the generated photons. Subsequently, we present the implemented scalable platform in which, by interfacing well-known OAM manipulation devices with the QD source, entangled intra- and interparticle states are generated in the hybrid Hilbert space composed of OAM and polarization.

2.1 Single-Photon Source

The single-photon source is a quantum-dot-based emitter embedded in an electrically controlled cavity on a commercially available Quandela e-Delight-LA photonic chip. A single self-assembled InGaAs QD is surrounded by a two Bragg reflectors made of $GaAs/Al_{0.95}Ga_{0.05}As$ $\lambda/4$ layers with 36 (16) pairs for the bottom (top) and positioned in the center of a micropillar.[63] The micropillar is connected to a larger circular structure that is electrically contacted, enabling the tuning of the emission frequency of the QD via the Stark effect. The sample is kept at 4 K in a low-vibration closed-cycle He cryostat Attocube - Attodry800. The QD source is pumped with a 79 MHz-pulsed laser shaped with a QShaper (Quandela) 4f pulse shaper to select a specific wavelength and achieve a bandwidth of ∼100 pm. The optical excitation of the QD is achieved in an LA phonon-assisted configuration with a laser at 927.2 nm blue-detuned from the transition,[83] which enables single-photon generation by exciton emission at (927.8 ± 0.2) nm [Fig. 2(a)]. The emitted photons are directly coupled in single-mode fiber (SMF) and spectrally separated from the residual pumping laser with bandpass filters. At the output of the e-Delight-LA system, we measure a single-photon count rate of $R_{\mathrm{det}} = 4$ MHz. The fibered brightness of the single-photon source depends mainly on the coupling efficiency into the SMF, the spectral separation transmission of the single-photon stream from the pump laser—whose effects we estimate in an overall efficiency of $\eta_{\mathrm{setup}} \sim 52\%$—and the detector efficiency, estimated to be around $\eta_{\mathrm{det}} \sim 38\%$. Using these figures, we estimate a first lens brightness of $B = \frac{R_{\mathrm{det}}}{R_{\mathrm{exc}}\eta_{\mathrm{det}}\eta_{\mathrm{setup}}} \sim 26\%$, where R_{exc} is the pump frequency. The overall quality of the single-photon generation can be characterized by measuring the multi-photon emission and indistinguishability. Using a standard Hanbury Brown and Twiss setup, we measured a second-order autocorrelation of $g^{(2)}(0) = (1.26 \pm 0.05)\%$. Such a figure is computed by normalizing the zero-time delay coincidences to the side peaks coincidences between two consecutive near-resonant excitations [Fig. 2(b)]. We also measured the indistinguishability between photons successively emitted by the QD, through an HOM interference experiment.[51] Two consecutively emitted photons are split by a beam splitter (BS) and coupled in SMFs, whose length

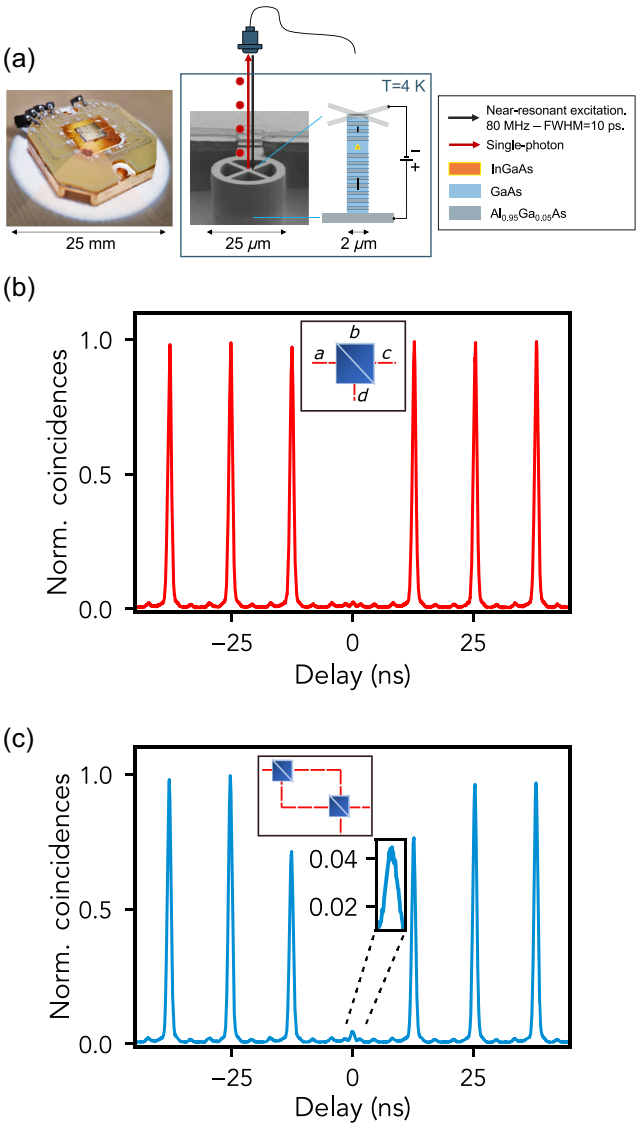

Fig. 2 Source HOM interference and second-order correlation function. (a) (Left) The single-photon source is a commercial device (Quandela): InGaAs quantum-dot based bright emitters are embedded in (right) electrically contacted micropillars. The source is pumped with a near-resonant ($\Delta\lambda = -0.6$ nm) FWHM 10 ps 79 MHz-pulsed laser (red arrow). The single photons (red dots) are emitted at a wavelength of 927.8 nm and are directly coupled to an SMF. (b) Through a standard Hanbury Brown and Twiss setup, we measure the second-order autocorrelation histogram of our QD-based source as a function of the delay. We obtain a single-photon purity of $g^{(2)}(0) = (1.26 \pm 0.05)\%$. (c) Normalized correlation histogram, obtained via an HOM interference experiment, through which we measure a two-photon interference fringe visibility between subsequent single photons emitted by the QD source of $V_{\mathrm{HOM}} = (93.05 \pm 0.06)\%$. Moreover, following Ref. 84, we obtain an indistinguishability value of $M_s = (95.5 \pm 0.1)\%$.

is chosen to delay one of them by ≈12.5 ns to ensure temporal overlap on a second BS. At its outputs, photons are collected in avalanche photodiode detectors (APDs) to record photon coincidence counts. Therefore, we evaluate a two-photon interference

visibility derived from the correlation histogram [Fig. 2(c)] as $V_{\mathrm{HOM}} = 1 - 2\frac{C_0}{\langle C\rangle_{t\to\infty}}$, where C_0 is the counts when the two photons are synchronized and $\langle C\rangle_{t\to\infty}$ is the average peak counts for relative temporal delays larger than one repetition rate of the laser. We measure an interference visibility $V_{\mathrm{HOM}} = (93.05 \pm 0.06)\%$, which can be corrected to account for unwanted multi-photon components,[84] resulting in a photon indistinguishability equal to $M_s = (95.5 \pm 0.1)\%$.

2.2 Experimental Implementation of OAM-Based Platform

We experimentally implemented a flexible platform for the study of single and multi-photon properties capable of implementing a probabilistic entangling quantum gate. A visual scheme of the setup is shown in Fig. 3.

For this purpose, the stream of single photons generated by the QD is preliminarily split through a fiber BS, and OAM encoding is performed separately on the two outputs. In particular, the input state, $|H,0\rangle$, having horizontal polarization and null OAM value, is selected through single mode fibers and polarizing beam splitters (PBSs). In the engineering stage, by placing a set of wave plates together with a q-plate on each arm, we are able to independently generate two distinct OAM-encoded single-photon states. In particular, a q-plate is a thin film of birefringent material (in our case, nematic liquid crystals) characterized by a nonuniform distribution of the optic axis across the plane transverse to the light propagation direction. The angle between the optic axis and the horizontal axis x of the device follows the relation $\alpha(\phi) = \alpha_0 + q\phi$, where ϕ is the azimuthal angle in the transverse plane, α_0 is the optic axis orientation for $\phi = 0$, and q is the topological charge, i.e., the winding number of the optic axis for $\phi \in [0,2\pi]$. Owing to the inhomogeneity of its optic axis distribution and to the resulting Pancharatnam–Berry geometric phases, the q-plate develops on the OAM degree of freedom of single photons an action that depends on their polarization, according to the following expression:[59,60]

$$\hat{Q} = \sum_m e^{-i2\alpha_0}|m-2q\rangle\langle m| \otimes |L\rangle\langle R| + e^{i2\alpha_0}|m+2q\rangle\langle m| \otimes |R\rangle\langle L|, \tag{1}$$

where $|R\rangle$ and $|L\rangle$ indicate right and left circular polarization states, respectively, and $|m\rangle$ represents the OAM value. The q-plates employed in the experiment are electrically tunable, i.e., they implement the operation $\hat{Q}_{\mathrm{exp}}(\delta) = \sin\frac{\delta}{2}\hat{Q} + \cos\frac{\delta}{2}\hat{\mathbb{I}}$, where $\hat{\mathbb{I}}$ is the identity operator and δ is the plate retardance that is controlled by applying an external voltage to the device. In the experiment, all the q-plates have $\delta = \pi$ in order to maximize the OAM-SAM conversion.

Therefore, an optical setup consisting of a quarter-wave plate (QWP), a half-wave plate (HWP), and a q-plate with $q = 1$, acting on the input state $|H,0\rangle$, is able to engineer arbitrary superpositions of $|L,-2\rangle$ and $|R,2\rangle$ as given by

$$|\Phi\rangle = \cos(\theta/2)|L,-2\rangle + e^{i\psi}\sin(\theta/2)|R,2\rangle, \tag{2}$$

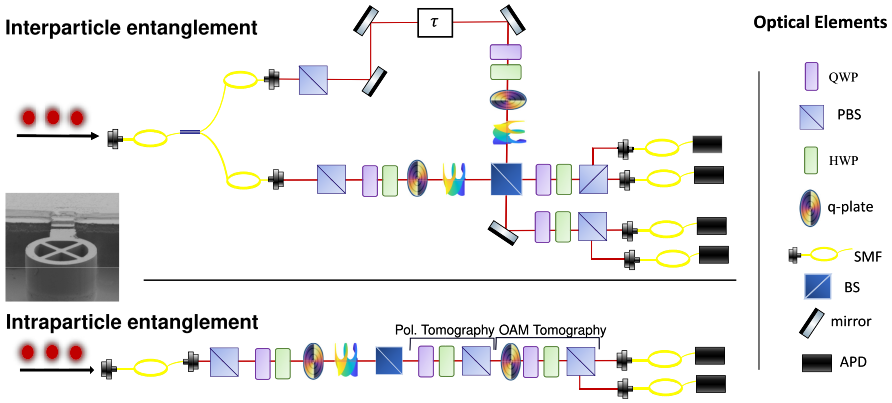

Fig. 3 Experimental setup. Single-photon states at a wavelength of 927.8 ± 0.2 nm are generated using a QD source pumped with a shaped 79 MHz-pulsed laser at 927.2 nm. Then, a fiber BS splits the photons between the two arms of the setup, and after passing through a PBS, the input states have horizontal polarization and OAM eigenvalue $m = 0$. In both paths, a series of QWP, HWP, and q-plate are used to produce OAM modes of the form reported in Eq. (2), while in one of the arms, a delay line (τ) is inserted in order to synchronize on the BS the photons emitted in different pulses of the pump beam. The intraparticle regime is investigated removing the fiber BS and performing all the experiment on a single line, involving the first input and output of the BS, as shown in the below panel. On the other hand, in the interparticle experiment, the photons are sent to the fiber BS, and the gate is implemented interfering on the second BS. After passing through the BS, the state of the photons is analyzed, coupled to SMFs and detected by APDs. The measurement setup consists in two different stages, a series of q-plate, QWP, HWP, and PBS are used to study the OAM states of the photons coupled with the polarization, while a QWP, an HWP, and a PBS compose the polarization analysis setup. In the interparticle regime, only OAM analysis is performed on the photon pairs, while in the intraparticle regime both analysis setups are used to separately investigate the polarization and OAM content of single photons, as shown in the lower panel.

where $\theta \in [0, \pi]$ and $\psi \in [0, 2\pi]$ can be set by properly orienting the optic axes of QWP and HWP. In this way, intrasystem entanglement between OAM and SAM degrees of freedom of single photons can be easily achieved. In particular, for $\theta = \pi/2$, the superpositions given in Eq. (2) correspond to the above mentioned VV states.

Subsequently, the two arms are synchronized by introducing a fixed delay in fiber and a tunable delay in air and then sent to a bulk BS used to probabilistically generate an entangled state between the two photons in the hybrid space of OAM and SAM by a postselection on the measured events.

Finally, in both single- and two-photon experiment, the state reconstruction is performed by using q-plates and polarization tomography setups comprising a QWP and an HWP followed by a PBS. In fact, the OAM tomography setup is implemented by adding a q-plate in front of the polarization tomography setup to convert the correlations present in the OAM degree of freedom on the polarization space [Eq. (1)]. The efficacy of this approach was demonstrated in Ref. 85 by exploiting pure-phase holograms displayed on photographic plates. In particular, in the intraparticle regime, the fiber BS is removed, and the entangled state is generated along the lower arm of the interferometer. Both the polarization and OAM analysis of such states is performed along one BS output by inserting the polarization tomography setups followed by the OAM tomography one. Instead, the analysis of the interparticle entangled state is performed by placing only the OAM tomography setups on each BS output. After the projection, the photons are collected in SMFs and detected using APDs. This scheme is used both to study the entanglement content of the states through Bell inequalities violation and to perform quantum state tomographies.

3 Entanglement Certification

In this section, we provide the theoretical description and report the results obtained studying the intraparticle and interparticle hybrid entanglement generated with the experimentally implemented platform. In all cases of interest, entanglement is certified through a violation of a CHSH Bell inequality and complete state tomography.

3.1 Vector Vortex Beam: Intrasystem Entanglement

The first investigation regards the generation of VV beams encoded into the single-photon states generated by the QD source. The VV beams are superpositions of two different OAM beams associated with orthogonal circular polarizations [see, for example, Eq. (2)]. Here, the two systems individuated by the OAM eigenstates $\{|-2\rangle, |2\rangle\}$ and the polarization states $\{|R\rangle, |L\rangle\}$ can be exploited for encoding two qubits. In this way, it is possible to define a complete basis of maximally entangled states between these two degrees of freedom. The set of Bell-like states is reported in Fig. 4, in which the nonuniform polarization distribution in the transverse plane is highlighted.

In our setup, to increase the generation rate, the signal is sent only in one of the two arms of the interferometer by removing the first fiber BS (see Fig. 3). The VV beams are prepared by making horizontally polarized photons passing subsequently through a QWP, an HWP, and a q-plate with $q = 1$. In this way, the state produced by the device is described by $\theta = \pi/2$ in Eq. (2) and a value of ψ which depends on the α_0 of the q-plate optic axis. This additional phase term is compensated by a further HWP (not shown in Fig. 3) in order to have $\psi = 0$. The final entangled state between OAM and polarization will be

$$|\Phi^+\rangle = \frac{1}{\sqrt{2}}(|L, -2\rangle + |R, 2\rangle). \tag{3}$$

Although such an entanglement structure is not associated with nonlocal properties (since it is encoded in a single carrier), these correlations can be detected using Bell-like inequalities. We refer to such type of quantum correlations as intraparticle entanglement.

The adoption of a nearly deterministic single-photon source allows us to perform the intraparticle analysis without the need of heralding measurements or postselection. The latter are

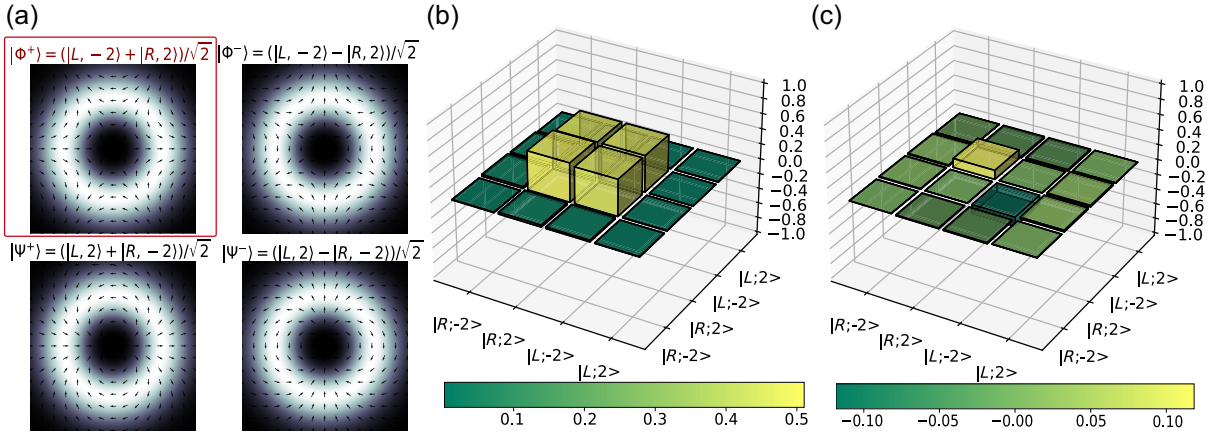

Fig. 4 Intraparticle entangled state: (a) intensity and polarization patterns of the Bell states basis in the combined OAM and polarization space. As highlighted by the red box, we focused our attention on the $|\Phi^+\rangle$ state. (b) Real and (c) imaginary parts of the measured density matrix for the $|\Phi^+\rangle$ state reconstructed via quantum state tomography. The fidelity between the reconstructed state and the theoretical one is equal to $\mathcal{F} = 0.9714 \pm 0.0007$, where the standard deviations are estimated through a Monte Carlo approach assuming a Poissonian statistics.

Table 1 Experimental results. The results are obtained both for the intraparticle and interparticle regimes. The measurement acquisition time T, the generation rate, the values for the Bell parameter (S), and the fidelity are reported. In particular, the violation $S^{(\text{raw})}$ is computed using raw data, while the parameter S is obtained by subtracting the background signal or the accidental coincidence. The fidelity value is computed by comparing the reconstructed density matrix with the triplet Bell state.

State	T (s)	Rate (Hz)	$S^{(\text{raw})}$	S	$\mathcal{F}$
Intra	20	99,000	2.736(8)	2.792(8)	0.9714(7)
Inter	400	146	2.516(6)	2.779(6)	0.935(2)

unavoidable procedures for generating single-photon states with high purity via probabilistic sources. This reduces drastically the losses allowing to reach a rate of ≃99 kHz of VV states generation (see the Supplementary Material for further details). The quality of the state and of its entanglement structure has been certified by the measurement stage setup shown and described in Sec. 2. In particular, we performed a quantum state tomography by analyzing the OAM and the polarization independently via cascaded measurement stages as in the lower panel of Fig. 3. The resulting density matrix is reported in Fig. 4, and the relative fidelity, computed by subtracting for dark counts, is $\mathcal{F} = 0.9714 \pm 0.0007$. Moreover, we also certified the intraparticle entanglement by evaluating a CHSH-like inequality. Collecting data for 20 s, we obtained a raw violation of $S^{(\text{raw})} = 2.736 \pm 0.008$, which exceeds the separable bound by 92 standard deviations, while the value obtained by subtracting the background signal is $S = 2.792 \pm 0.008$, which exceeds the classical bound by 99 standard deviations. The results are summarized in Table 1.

3.2 Certification of Photon States Generation

In quantum information processes, an important computational resource relies on the capability of manipulating multiple photons and making them interact. Therefore, in this section, we assess the capacity of codifying specific OAM states on photons generated by subsequent pulsed pumping of the QD. This is performed by evaluating the visibility of HOM interference in a BS, which is equivalent to a pairwise overlap estimation in a SWAP test.[86] There are some previous examples of HOM experiments with single-photon states carrying OAM,[39,87] but our tests are among the first to be applied to vector beams generated by a deterministic single-photon source.

Let us first briefly review the effect of an unbiased BS on the field annihilation and creation operators, $\hat{a}, \hat{a}^\dagger$ and $\hat{b}, \hat{b}^\dagger$. The relation between input modes $\{a, b\}$ and output modes $\{c, d\}$ can be expressed as (Fig. 2)

$$\hat{a}^\dagger \mapsto \frac{1}{\sqrt{2}}(\hat{c}^\dagger - \hat{d}^\dagger), \hat{b}^\dagger \mapsto \frac{1}{\sqrt{2}}(\hat{c}^\dagger + \hat{d}^\dagger). \tag{4}$$

By considering two photons at the two inputs of the BS, the signature of the interference is a change in the probability to detect photons in different outputs (see the Supplementary Material). In particular, two photons are indistinguishable if their states, associated with each degree of freedom, are the same from the point of view of the observer. To approach this condition in our setup, a delay line is used to synchronize the photons in the temporal domain. This is mandatory because the two single photons are emitted by the QD at different times. However, when the photons are characterized by an OAM value different from zero and superposed polarizations, it is necessary to take into account the effect of reflections. Indeed, in a physical BS, the semireflective mirror flips the elicity of both OAM and polarization. In other words, after one reflection, we have $\{|R\rangle, |L\rangle\} \to \{|L\rangle, |R\rangle\}$ and $|\pm 2\rangle \to |\mp 2\rangle$, while horizontal and vertical polarizations are eigenstates of this operation with eigenvalues of opposite signs. Then, we have that the creation operators are changed as follows:

$$\begin{aligned}
&\hat{a}_R^\dagger, \hat{b}_R^\dagger \mapsto \frac{1}{\sqrt{2}}(\hat{c}_R^\dagger - \hat{d}_L^\dagger), \quad \frac{1}{\sqrt{2}}(\hat{c}_L^\dagger + \hat{d}_R^\dagger),\\
&\hat{a}_L^\dagger, \hat{b}_L^\dagger \mapsto \frac{1}{\sqrt{2}}(\hat{c}_L^\dagger - \hat{d}_R^\dagger), \quad \frac{1}{\sqrt{2}}(\hat{c}_R^\dagger + \hat{d}_L^\dagger),\\
&\hat{a}_m^\dagger, \hat{b}_m^\dagger \mapsto \frac{1}{\sqrt{2}}(\hat{c}_m^\dagger - \hat{d}_{-m}^\dagger), \quad \frac{1}{\sqrt{2}}(\hat{c}_{-m}^\dagger + \hat{d}_m^\dagger).
\end{aligned} \tag{5}$$

Since the indistinguishability of photons generated by the source has already been checked in Sec. 2.1, here we are interested in computing the overlap between VV states encoded in different photons. As for the previous analysis, the OAM and polarization degrees of freedom are controlled through a series of QWP, HWP, and q-plate placed in each arm of the interferometer. This allows us to prepare the desired state for each photon.

Considering the BS action in Eq. (5), we expect no interference when the two photons are prepared as $|R, 2\rangle_a |R, 2\rangle_b$, since the reflected beam and the transmitted one in the outputs c and d will display orthogonal states. Conversely, the HOM effect occurs when the initial state is $|R, 2\rangle_a |L, -2\rangle_b$. The correlation histograms, obtained via an HOM interference experiment, for both input states $|R, 2\rangle_a |R, 2\rangle_b$ and $|R, 2\rangle_a |L, -2\rangle_b$ are reported in Figs. 5(a) and 5(b). The visibility of such HOM experiments quantifies the variation, from the maximum to minimum overlapping between the wave functions, of the probability of detecting photons in different outputs. The obtained visibilities are $V_{|R,2\rangle,|R,2\rangle} = -4\% \pm 1\%$ and $V_{|R,2\rangle,|L,-2\rangle} = 90.1\% \pm 0.3\%$, respectively. We repeat the same interference scheme with VV states, such as $|\Phi^+\rangle$ and $|\Phi^-\rangle$ (see Fig. 4). For these classes of states, we note that they are symmetric with respect to the BS operation. This means that the reflected photon and the transmitted one always display the same state if they are indistinguishable at the input faces of the BS (see the Supplementary Material). The resulting HOM correlations for the input state $|\Phi^+\rangle_a |\Phi^-\rangle_b$ are reported in Fig. 5(c) and the achieved visibility is equal to $V_{|\Phi^+\rangle,|\Phi^-\rangle} = 0.70\% \pm 0.10\%$, as expected. On the contrary, when the two photons are prepared in the same VV states such as $|\Phi^+\rangle_a |\Phi^+\rangle_b$, the theoretical HOM visibility is 1. We measured $V_{|\Phi^+\rangle,|\Phi^+\rangle} = 88.2\% \pm 0.3\%$, as reported in Fig. 5(d).

A further peculiar configuration is when the interfering input states are neither equal nor orthogonal, for which we expect a $V = \frac{1}{2}$. This is the case of two photons prepared in the input ports as $|\Phi^+\rangle_a |R, 2\rangle_b$. The measured visibility is $V_{|\Phi^+\rangle,|R,2\rangle} = 44.5\% \pm 0.6\%$ [Fig. 5(e)].

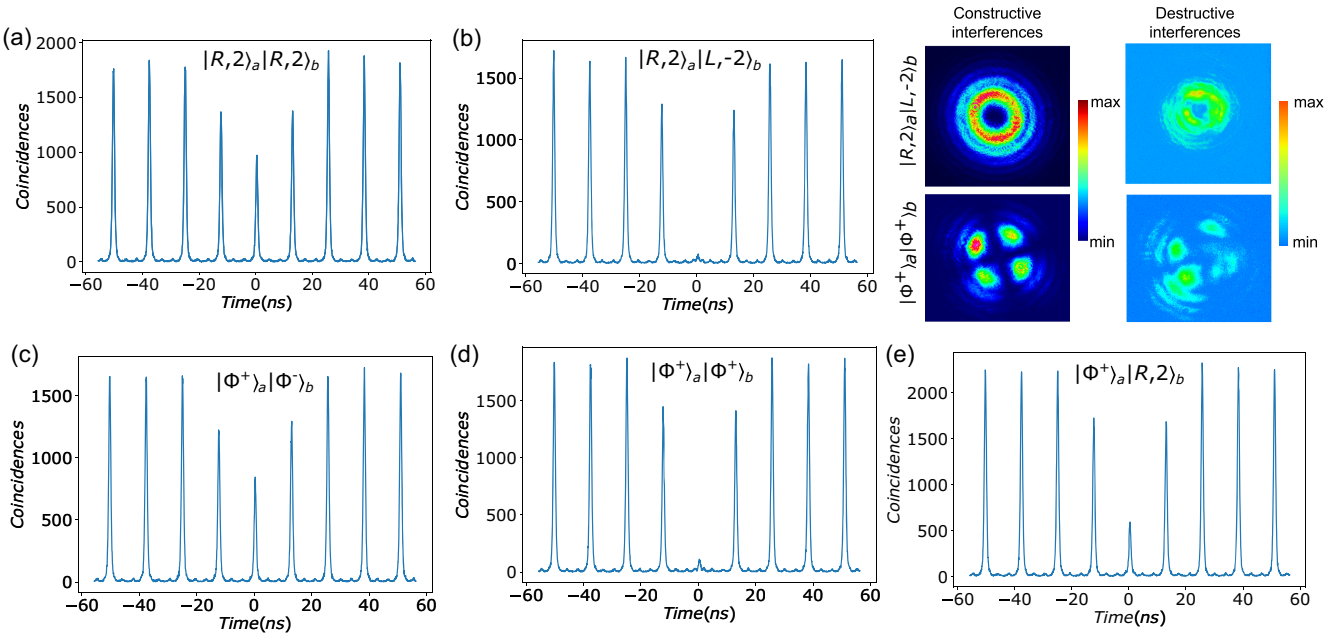

Fig. 5 HOM interference for OAM states: measured coincidences at the output of the final BS, see Fig. 3, for different input states in the hybrid space of OAM and polarization. A perfect HOM interference can be obtained only when the photon states are indistinguishable from the point of view of the observer. By knowing the BS action on circular polarization and OAM (see the Supplementary Material), we observe a near-unitary visibility when the photons are prepared in the same eigenstate of the BS reflection operation $|\Phi^+\rangle_a|\Phi^+\rangle_b$ (panel d), or when the initial states have opposite circular polarization and OAM value [panel (b)]; while near-zero visibility is reported in panels (a) and (c) for initial states $|R,2\rangle_a|R,2\rangle_b$ and $|\Phi^+\rangle_a|\Phi^-\rangle_b$, respectively. Moreover, we also analyze the hybrid configuration in which one photon is prepared in the state $|R,2\rangle$ and the other in the VV state $|\Phi^+\rangle$. In the latter case, the expected number of coincidences is half of the one obtained for distinguishable photons [panel (e)]. The reported intensity patterns are associated to constructive and destructive interference for both initial states $|R,2\rangle_a|L,-2\rangle_b$ and $|\Phi^+\rangle_a|\Phi^+\rangle_b$.

3.3 Two-Photon Quantum Gate: Intersystem Entanglement

The configuration described in the previous section can be exploited to implement a multi-qubit probabilistic quantum gate able to generate an entangled state in the hybrid space composed by OAM and polarization. In particular, by postselecting on the two-photon coincidence events resulting from the preparation $|R,2\rangle_a|R,2\rangle_b$, and noticing that one of the outputs is affected by a further reflection that introduces a phase π between horizontal and vertical polarization, and inverts the OAM value, the following state is generated:

$$|\Phi\rangle = \frac{|L,-2\rangle_c|R,2\rangle_d + |R,2\rangle_c|L,-2\rangle_d}{\sqrt{2}} = \frac{|1,0\rangle|0,1\rangle + |0,1\rangle|1,0\rangle}{\sqrt{2}}, \tag{6}$$

where we took off the direction subscript $\{c,d\}$ and we identified $|L,-2\rangle = |1,0\rangle$ and $|R,2\rangle = |0,1\rangle$. Therefore, the generated state is entangled in the space spanned by the tensor product of the four-dimensional (4D) qudits encoded in the combined OAM and polarization degrees of freedom for each photon. However, in the hybrid OAM-SAM space, this state can also be considered equivalent to a two-dimensional (2D) maximally entangled state. Indeed, relabeling the state $|L,-2\rangle$ as qubit $|0\rangle$ and the state $|R,2\rangle$ as qubit $|1\rangle$, the state in Eq. (6) turns out to be equivalent to a triplet Bell state,

$$|\Phi\rangle = \frac{|L,-2\rangle_c|R,2\rangle_d + |R,2\rangle_c|L,-2\rangle_d}{\sqrt{2}} = \frac{|0\rangle|1\rangle + |1\rangle|0\rangle}{\sqrt{2}}. \tag{7}$$

Therefore, this state exhibits quantum correlations that could be detected by performing a Bell-like test that is used as an entanglement witness. In particular, we evaluated a CHSH-like inequality performing the projective measurements placing the OAM measurement stage, shown in Fig. 3, on both BS outputs. Collecting data for 400 s and with a coincidence rate of 146 Hz, we obtained a raw violation of $S^{(\mathrm{raw})} = 2.516 \pm 0.006$, which exceeds the classical bound by 86 standard deviations. The value obtained by subtracting the accidental coincidences, mainly due to background noise and quantified measuring coincidences between signals in the region between two consecutive peaks (with a relative delay of ∼6 ns), is $S = 2.779 \pm 0.006$, which exceeds the separable bound by 130 standard deviations.

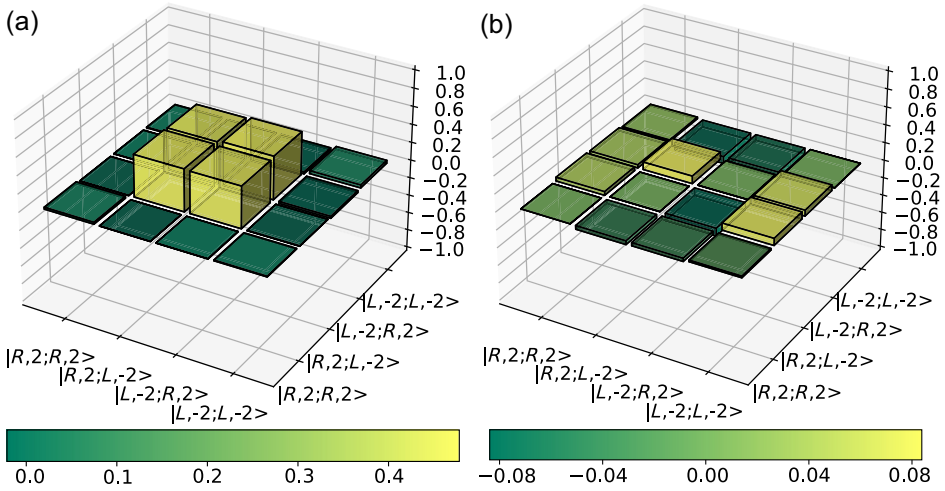

Fig. 6 Interparticle entangled state. (a) Real and (b) imaginary parts of the measured density matrix for the two-photon state in the hybrid OAM-polarization space reported in Eq. (7), these are reconstructed via quantum state tomography. The fidelity between the reconstructed state and the theoretical one is equal to $\mathcal{F} = 0.935 \pm 0.002$, where the standard deviation is estimated through a Monte Carlo approach assuming a Poissonian statistics.

Moreover, we also performed a quantum state tomography of the state using the same experimental configuration. The measurement apparatus selects on the 4D subspace $\{|R,2\rangle_1, |L,-2\rangle_1\} \otimes \{|R,2\rangle_2, |L,-2\rangle_2\}$ in which the interparticle entangled state lives. In fact, it contains the significantly nonzero elements of the whole density matrix of the states. Other terms outside such a subspace come from the imperfect conversion of the OAM by the q-plates. The probability of such components in the state can be kept very low, and thus can be neglected, by tuning the δ parameters of the q-plates toward the π value. Subtracting for accidental coincidences, the estimated fidelity changes from $\mathcal{F}^{(\mathrm{raw})} = 0.869 \pm 0.002$ to $\mathcal{F} = 0.935 \pm 0.002$. The retrieved density matrix is shown in Fig. 6. The results are summarized in Table 1. It is worth noting that the decrease in the coincidence rate is mainly due to the coupling efficiency into SMFs in the detection stage of about 45% (see the Supplementary Material for further details). This lower value depends on both the limited conversion efficiency of the QPs and on the higher divergence to which beams endowed with OAM are subjected. Other loss effects that need to be included are the q-plate transmission of about 75% acting on each photon. Therefore, looking toward gates with more than two photons, where the weight of the losses increases exponentially in the number of photons, the rate could be improved by compensating for losses due to the divergence and adopting experimental devices with limited losses.

4 Conclusions

In this paper, we experimentally implemented a platform capable of generating on-demand photonic quantum states in high-dimensional Hilbert spaces. This was achieved by combining a bright QD source with q-plates, devices capable of coupling OAM and polarization of single photons, placed in an interferometric configuration. After assessing the properties of the source, such as the multi-photon component, and the indistinguishability of the emitted photons, we focused on the generation and analysis of entangled states in the hybrid space composed of OAM and polarization. The setup allows us to study both the intra- and interparticle entanglement. For the former, we generated a VV state using only the engineering stage placed in one arm of the interferometer, while for the latter we exploited the interference between modulated single photons generated by the QD in two consecutive excitations to implement a probabilistic quantum gate capable of producing entangled two-photon states. The characterization of the interferometer scheme was preliminarily performed by evaluating the overlap between quantum states of single photons encoded in the hybrid Hilbert space. In particular, we observed high HOM visibilities for single photons that turn out to be indistinguishable in the detection stage, while very low visibility was observed for orthogonal quantum states. The qualities of both intra- and interparticle hybrid entangled states were evaluated by performing quantum state tomography and using Bell tests to estimate the CHSH inequality. The high values of fidelities and inequality violations highlight the performance of the proposed setup for the engineering of high-dimensional entangled states.

In summary, we proposed and implemented experimentally a flexible platform able to generate both nearly deterministic single-photon states that exhibit entanglement between OAM and SAM degrees of freedom and two-photon entangled states. The employed simple and effective scheme could be extended to the multi-photon regime, opening the way to high-dimensional multi-photon experiments, whose scalability is extremely demanding for platforms based on probabilistic sources. In conclusion, the results demonstrated in the present paper can provide advances both for fundamental investigations and quantum photonic applications.

Code, Data, and Materials Availability

Data underlying the results presented in this paper may be obtained from the authors upon reasonable request.

Acknowledgments

This work was supported by the European Union's Horizon 2020 Research and Innovation Programme under the PHOQUSING Project GA No. 899544, and the European Union's Horizon 2020 Research and Innovation Programme QUDOT-TECH under the Marie Sklodowska-Curie Grant Agreement No. 86109. The authors declare no conflicts of interest.

References

1. H. Rubinsztein-Dunlop et al., "Roadmap on structured light," *J. Opt.* **19**, 013001 (2016).
2. L. Allen et al., "Orbital angular momentum of light and the transformation of Laguerre-Gaussian laser modes," *Phys. Rev. A* **45**, 8185–8189 (1992).
3. M. P. Lavery et al., "Detection of a spinning object using light's orbital angular momentum," *Science* **341**(6145), 537–540 (2013).
4. L. Torner, J. P. Torres, and S. Carrasco, "Digital spiral imaging," *Opt. Express* **13**, 873–881 (2005).
5. D. S. Simon and A. V. Sergienko, "Two-photon spiral imaging with correlated orbital angular momentum states," *Phys. Rev. A* **85**, 043825 (2012).
6. N. Uribe-Patarroyo et al., "Object identification using correlated orbital angular momentum states," *Phys. Rev. Lett.* **110**, 043601 (2013).
7. Q. Zhan, "Trapping metallic Rayleigh particles with radial polarization," *Opt. Express* **12**, 3377–3382 (2004).
8. A. E. Willner et al., "Optical communications using orbital angular momentum beams," *Adv. Opt. Photonics* **7**, 66 (2015).
9. M. Malik et al., "Influence of atmospheric turbulence on optical communications using orbital angular momentum for encoding," *Opt. Express* **20**(12), 13195–13200 (2012).
10. J. Wang et al., "Terabit free-space data transmission employing orbital angular momentum multiplexing," *Nat. Photonics* **6**, 488–496 (2012).
11. J. Baghdady et al., "Multi-gigabit/s underwater optical communication link using orbital angular momentum multiplexing," *Opt. Express* **24**(9), 9794–9805 (2016).
12. N. Bozinovic et al., "Terabit-scale orbital angular momentum mode division multiplexing in fibers," *Science* **340**, 1545–1548 (2013).
13. G. Gibson et al., "Free-space information transfer using light beams carrying orbital angular momentum," *Opt. Express* **12**(22), 5448–5456 (2004).
14. M. Krenn et al., "Twisted light transmission over 143 km," *Proc. Natl. Acad. Sci. U. S. A.* **113**, 13648–13653 (2016).
15. D. Cozzolino et al., "High-dimensional quantum communication: benefits, progress, and future challenges," *Adv. Quantum Technol.* **2**(12), 1900038 (2019).
16. M. Krenn et al., "Twisted photon entanglement through turbulent air across Vienna," *Proc. Natl. Acad. Sci. U. S. A.* **112**(46), 14197–14201 (2015).
17. M. Malik et al., "Multi-photon entanglement in high dimensions," *Nat. Photonics* **10**, 248–252 (2016).
18. D. Cozzolino et al., "Air-core fiber distribution of hybrid vector vortex-polarization entangled states," *Adv. Photonics* **1**(4), 046005 (2019).
19. Y. Zhou et al., "Using all transverse degrees of freedom in quantum communications based on a generic mode sorter," *Opt. Express* **27**(7), 10383–10394 (2019).
20. X.-L. Wang et al., "Quantum teleportation of multiple degrees of freedom of a single photon," *Nature* **518**, 516–519 (2015).
21. M. Mirhosseini et al., "High-dimensional quantum cryptography with twisted light," *New J. Phys.* **17**, 033033 (2015).
22. A. Sit et al., "High-dimensional intracity quantum cryptography with structured photons," *Optica* **4**, 1006–1010 (2017).
23. F. Bouchard et al., "Quantum cryptography with twisted photons through an outdoor underwater channel," *Opt. Express* **26**, 22563–22573 (2018).
24. F. Cardano et al., "Statistical moments of quantum-walk dynamics reveal topological quantum transitions," *Nat. Commun.* **7**, 11439 (2016).
25. F. Cardano et al., "Detection of Zak phases and topological invariants in a chiral quantum walk of twisted photons," *Nat. Commun.* **8**, 15516 (2017).
26. I. Buluta and F. Nori, "Quantum simulators," *Science* **326**(5949), 108–111 (2009).
27. B. P. Lanyon et al., "Simplifying quantum logic using higher-dimensional Hilbert spaces," *Nat. Phys.* **5**, 134–140 (2009).
28. T. C. Ralph, K. J. Resch, and A. Gilchrist, "Efficient Toffoli gates using qudits," *Phys. Rev. A* **75**, 022313 (2007).
29. B. Hiesmayr, M. De Dood, and W. Löffler, "Observation of four-photon orbital angular momentum entanglement," *Phys. Rev. Lett.* **116**(7), 073601 (2016).
30. H. Bechmann-Pasquinucci and A. Peres, "Quantum cryptography with 3-state systems," *Phys. Rev. Lett.* **85**(15), 3313–3316 (2000).
31. L. Sheridan and V. Scarani, "Security proof for quantum key distribution using qudit systems," *Phys. Rev. A* **82**(3), 030301 (2010).
32. A. Aiello et al., "Quantumlike nonseparable structures in optical beams," *New J. Phys.* **17**, 043024 (2015).
33. M. Li et al., "Transverse spinning of particles in highly focused vector vortex beams," *Phys. Rev. A* **95**(5), 053802 (2017).
34. F. Cardano and L. Marrucci, "Spin-orbit photonics," *Nat. Photonics* **9**, 776–778 (2015).
35. G. Vallone et al., "Free-space quantum key distribution by rotation-invariant twisted photons," *Phys. Rev. Lett.* **113**(6), 060503 (2014).
36. V. D'Ambrosio et al., "Complete experimental toolbox for alignment-free quantum communication," *Nat. Commun.* **3**, 961 (2012).
37. S. Slussarenko et al., "Universal unitary gate for single-photon spin-orbit four-dimensional states," *Phys. Rev. A* **80**, 022326 (2009).
38. E. Nagali et al., "Polarization control of single photon quantum orbital angular momentum states," *Opt. Express* **17**, 18745–18759 (2009).
39. E. Nagali et al., "Optimal quantum cloning of orbital angular momentum photon qubits through Hong–Ou–Mandel coalescence," *Nat. Photonics* **3**, 720–723 (2009).
40. L.-P. Deng, H. Wang, and K. Wang, "Quantum CNOT gates with orbital angular momentum and polarization of single-photon quantum logic," *J. Opt. Soc. Am. B* **24**, 2517–2520 (2007).
41. Y. Chen et al., "Mapping twisted light into and out of a photonic chip," *Phys. Rev. Lett.* **121**(23), 233602 (2018).
42. B. P. da Silva et al., "Spin–orbit laser mode transfer via a classical analogue of quantum teleportation," *J. Phys. B Atomic Mol. Opt. Phys.* **49**, 055501 (2016).
43. V. Parigi et al., "Storage and retrieval of vector beams of light in a multiple-degree-of-freedom quantum memory," *Nat. Commun.* **6**(1), 7706 (2015).
44. T. Giordani et al., "Machine learning-based classification of vector vortex beams," *Phys. Rev. Lett.* **124**(16), 160401 (2020).
45. A. R. C. Pinheiro et al., "Vector vortex implementation of a quantum game," *J. Opt. Soc. Am. B* **30**, 3210–3214 (2013).
46. Y. Kozawa, D. Matsunaga, and S. Sato, "Superresolution imaging via superoscillation focusing of a radially polarized beam," *Optica* **5**(2), 86–92 (2018).
47. A. Suprano et al., "Propagation of structured light through tissue-mimicking phantoms," *Opt. Express* **28**(24), 35427–35437 (2020).
48. E. Polino et al., "Photonic quantum metrology," *AVS Quantum Sci.* **2**(2), 024703 (2020).
49. R. Fickler et al., "Quantum entanglement of high angular momenta," *Science* **338**(6107), 640–643 (2012).

50. S. Berg-Johansen et al., "Classically entangled optical beams for high-speed kinematic sensing," *Optica* **2**(10), 864–868 (2015).
51. C. K. Hong, Z. Y. Ou, and L. Mandel, "Measurement of subpicosecond time intervals between two photons by interference," *Phys. Rev. Lett.* **59**(18), 2044–2046 (1987).
52. F. Bouchard et al., "Two-photon interference: the Hong–Ou–Mandel effect," *Rep. Progr. Phys.* **84**, 012402 (2020).
53. E. Karimi et al., "Exploring the quantum nature of the radial degree of freedom of a photon via Hong-Ou-Mandel interference," *Phys. Rev. A* **89**, 013829 (2014).
54. Y. Zhang et al., "Hong-Ou-Mandel interference of entangled hermite-Gauss modes," *Phys. Rev. A* **94**, 033855 (2016).
55. M. Hiekkamäki and R. Fickler, "High-dimensional two-photon interference effects in spatial modes," *Phys. Rev. Lett.* **126**(12), 123601 (2021).
56. B. Chen et al., "Bright solid-state sources for single photons with orbital angular momentum," *Nat. Nanotechnol.* **16**(3), 302–307 (2021).
57. R. Fickler et al., "Real-time imaging of quantum entanglement," *Sci. Rep.* **3**(1), 1914 (2013).
58. E. Yao et al., "Observation of quantum entanglement using spatial light modulators," *Opt. Express* **14**, 13089–13094 (2006).
59. L. Marrucci, C. Manzo, and D. Paparo, "Optical spin-to-orbital angular momentum conversion in inhomogeneous anisotropic media," *Phys. Rev. Lett.* **96**(16), 163905 (2006).
60. L. Marrucci et al., "Spin-to-orbital conversion of the angular momentum of light and its classical and quantum applications," *J. Opt.* **13**, 064001 (2011).
61. T. Stav et al., "Quantum entanglement of the spin and orbital angular momentum of photons using metamaterials," *Science* **361**(6407), 1101–1104 (2018).
62. G. Brassard et al., "Limitations on practical quantum cryptography," *Phys. Rev. Lett.* **85**(6), 1330–1333 (2000).
63. N. Somaschi et al., "Near-optimal single-photon sources in the solid state," *Nat. Photonics* **10**, 340–345 (2016).
64. H. Wang et al., "Towards optimal single-photon sources from polarized microcavities," *Nat. Photonics* **13**, 770–775 (2019).
65. R. Uppu et al., "Scalable integrated single-photon source," *Sci. Adv.* **6**(50), eabc8268 (2020).
66. N. Tomm et al., "A bright and fast source of coherent single photons," *Nat. Nanotechnol.* **16**(4), 399–403 (2021).
67. E. Waks et al., "Quantum cryptography with a photon turnstile," *Nature* **420**(6917), 762 (2002).
68. R. Collins et al., "Quantum key distribution system in standard telecommunications fiber using a short wavelength single photon source," *J. Appl. Phys.* **107**(7), 073102 (2010).
69. J.-P. Li et al., "Multiphoton graph states from a solid-state single-photon source," *ACS Photonics* **7**(7), 1603–1610 (2020).
70. D. Istrati et al., "Sequential generation of linear cluster states from a single photon emitter," *Nat. Commun.* **11**(1), 5501 (2020).
71. J.-P. Li et al., "Heralded nondestructive quantum entangling gate with single-photon sources," *Phys. Rev. Lett.* **126**(14), 140501
(2021).
72. A. Dousse et al., "Ultrabright source of entangled photon pairs," *Nature* **466**(7303), 217–220 (2010).
73. K. Takemoto et al., "Quantum key distribution over 120 km using ultrahigh purity single-photon source and superconducting single-photon detectors," *Sci. Rep.* **5**(1), 14383 (2015).
74. T. Giordani et al., "Experimental engineering of arbitrary qudit states with discrete-time quantum walks," *Phys. Rev. Lett.* **122**(2), 020503 (2019).
75. A. Suprano et al., "Dynamical learning of a photonics quantum-state engineering process," *Adv. Photonics* **3**(6), 066002 (2021).
76. V. D'Ambrosio et al., "Entangled vector vortex beams," *Phys. Rev. A* **94**, 030304 (2016).
77. E. Karimi et al., "Spin-orbit hybrid entanglement of photons and quantum contextuality," *Phys. Rev. A* **82**, 022115 (2010).
78. D. Huber et al., "Strain-tunable GAAS quantum dot: a nearly dephasing-free source of entangled photon pairs on demand," *Phys. Rev. Lett.* **121**(3), 033902 (2018).
79. J. Torres, A. Alexandrescu, and L. Torner, "Quantum spiral bandwidth of entangled two-photon states," *Phys. Rev. A* **68**(5), 050301 (2003).
80. S. P. Walborn et al., "Spatial correlations in parametric down-conversion," *Phys. Rep.* **495**, 87–139 (2010).
81. N. H. Valencia et al., "Entangled ripples and twists of light: radial and azimuthal Laguerre–Gaussian mode entanglement," *J. Opt.* **23**(10), 104001 (2021).
82. Y. H. Shih and C. O. Alley, "New type of Einstein–Podolsky–Rosen–Bohm experiment using pairs of light quanta produced by optical parametric down conversion," *Phys. Rev. Lett.* **61**(26), 2921–2924 (1988).
83. S. E. Thomas et al., "Bright polarized single-photon source based on a linear dipole," *Phys. Rev. Lett.* **126**(23), 233601 (2021).
84. H. Ollivier et al., "Hong-Ou-Mandel interference with imperfect single photon sources," *Phys. Rev. Lett.* **126**(6), 063602 (2021).
85. E. Nagali et al., "Quantum information transfer from spin to orbital angular momentum of photons," *Phys. Rev. Lett.* **103**(1), 013601 (2009).
86. J. C. Garcia-Escartin and P. Chamorro-Posada, "Swap test and Hong-Ou-Mandel effect are equivalent," *Phys. Rev. A* **87**, 052330 (2013).
87. B. Ndagano and A. Forbes, "Entanglement distillation by Hong-Ou-Mandel interference with orbital angular momentum states," *APL Photonics* **4**(1), 016103 (2019).

Alessia Suprano received her PhD in physics in 2022. She is currently a post doc in the Physics Department at Sapienza University of Rome. Her current interests are focused on high-dimensional quantum information protocols in particular, for the implementation and exploitation of quantum walks in the orbital angular momentum degree of freedom of photons and for the study of nonlocality in networks.

Danilo Zia is a PhD student in the Quantum Information Laboratory of Pr. Fabio Sciarrino. Currently, he is investigating the applications of quantum walk dynamics in the orbital angular momentum degree of freedom of the photons using machine learning techniques. He graduated in October 2020 from Sapienza Università di Roma.

Mathias Pont studied theoretical physics and applied mathematics at Ecole Polytechnique in Paris. He joined Pr. S. Francoeur's research group at Polytechnique Montreal to work on the resonant excitation of Te isoelectronic centers in ZnSe for quantum information applications. He then pursued a doctoral degree in P. Senellart's group at C2N in Paris to work on interfacing bright QD single-photon source with integrated photonic circuits. He is now working at Quandela as a research information scientist.

Taira Giordani received her PhD in physics in 2020. She is currently a researcher in the Physics Department at Sapienza University of Rome. Her research focuses on the experimental implementation of quantum walks in integrated photonic devices and the angular momentum of light. In this context, her efforts aim to develop machine learning and optimization methods for the certification and engineering of photonic quantum walks platforms.

Giovanni Rodari is a PhD student in the Quantum Information Laboratory of Pr. Fabio Sciarrino. His main research interests are related to foundational themes—nonclassicality, causality—together with the investigation and implementation of quantum information protocols on photonis-based platforms. He graduated in October 2021 from Sapienza Università di Roma.

Mauro Valeri received his PhD in 2021 with a thesis entitled "Photonics technologies for quantum communication and metrology." The research activity of Mauro Valeri involved the study of quantum technology for quantum communication and metrology. During his PhD, he developed integrated and bulk sources of entangled photons to be distributed in quantum networks and exploited for quantum information protocols.

Bruno Piccirillo is professor of physics at the University of Naples "Federico II." His expertise ranges from nonlinear optics to microfluidics, optical interferometry, angular momentum of light, quantum optics, etc. He is currently interested in shaping and sensing wavefront and polarization of electromagnetic radiation. His main achievements include the first demonstration of photon OAM transfer from light to transparent media without topological defects (2001), the first electrically driven q-plate, the first geometric phase-based shearing interferometer.

Gonzalo Carvacho obtained his PhD from the University of Rome in 2018 with a thesis entitled "Multiphoton hybrid systems and their applications in quantum information and quantum communication." He is currently a lecturer in the Physics Department at Sapienza University of Rome and his research activities are focused on quantum causality, quantum communication and multiphoton dynamics by exploiting bulk optics, photonic integrated devices and G/Q-plates for structured light.

Nicolò Spagnolo received his PhD in 2012 in physical sciences of matter with a thesis on experimental multiphoton quantum optical states. He is currently a tenure-track assistant professor in the Physics Department of Sapienza Università di Roma. His research interests are focused on quantum information protocols employing different photonic platforms. These research activities include the implementation of boson sampling instances and of validation protocols with integrated photonics, quantum phase estimation experiments, and optical quantum communications.

Pascale Senellart obtained her PhD from University Paris 6 in 2001 for her studies on microcavity polaritons. After two postdoctoral positions in industrial laboratories, she joined the CNRS at the end of 2002 at the Laboratoire de Photonique et de Nanostructures where she started a research line on cavity quantum electrodynamics with semiconductor quantum dots. Her main field of research is solid-state quantum physics.

Lorenzo Marrucci is professor of physics at the University of Naples. He has coauthored over 200 scientific articles and 5 patents in optics and photonics. He is well known for his invention of the "q-plate," a device that allows generating orbital angular momentum from polarization manipulations. He has coordinated several international research projects, including an ERC Advanced Grant. He has also held various academic-management positions; currently he is vice rector for research at the University of Naples.

Fabio Sciarrino received his PhD in 2004 with a thesis in experimental quantum optics. He is a full professor and head of the Quantum Information Lab in the Department of Physics of Sapienza Università di Roma. Since 2013, he has been a fellow of the Sapienza School for Advanced Studies. His main field of research is quantum information and quantum optics, with works on quantum teleportation, optimal quantum machines, fundamental tests, quantum communication, and orbital angular momentum.